

PAPER • OPEN ACCESS

Time-gated Raman spectroscopy for biomedical application under ambient or strong background light conditions

To cite this article: Christopher Corden *et al* 2021 *J. Phys. D: Appl. Phys.* **54** 504003

View the [article online](#) for updates and enhancements.

You may also like

- [Identification of the spintronic \$\text{Ni}_{0.2}\text{V}_{0.8}\$ center in c-GaN and its qubit applications](#)
Ruixia Gao, Guodong Bian, Heng Yuan et al.
- [Time-gated Raman spectroscopy – a review](#)
Martin Kögler and Bryan Heilala
- [Fabrication of ultra-shallow junction by *in situ* doped amorphous silicon films and its application in silicon drift detectors](#)
Shuai Jiang, Rui Jia, Ke Tao et al.



IOP | ebooks™

Bringing together innovative digital publishing with leading authors from the global scientific community.

Start exploring the collection—download the first chapter of every title for free.

Time-gated Raman spectroscopy for biomedical application under ambient or strong background light conditions

Christopher Corden, Radu Boitor and Ioan Notingher* 

School of Physics and Astronomy, University Park, University of Nottingham, NG7 2RD Nottingham, United Kingdom

E-mail: ioan.notingher@nottingham.ac.uk

Received 17 May 2021, revised 6 September 2021

Accepted for publication 16 September 2021

Published 28 September 2021



CrossMark

Abstract

Many biomedical applications require measurements of Raman spectra of tissue under ambient lighting conditions. However, the background light often swamps the weaker Raman signal. The use of time-gated (TG) Raman spectroscopy based on a single photon avalanche diode (SPAD) operating in time-correlated single photon counting and near-infrared laser excitation was investigated for acquisition of Raman spectra and spectral images of biological tissue. The results obtained using animal tissue samples (adipose tissue and muscle) show that the time gating modality enables measurement of Raman spectra under background light conditions of similar quality as conventional continuous wave Raman spectroscopy in the absence of background light. Optimal suppression of the background light was observed for time gate widths of 300–1000 ps. The results also showed that TG Raman spectroscopy was able to detect subtle spectral differences required for medical diagnostics, such as differences in Raman spectra of cancer and normal tissue. While the current instrument required scanning of the grating in order to obtain full Raman spectra, leading to impractical times for multi-wavenumber Raman mapping, imaging time could be drastically reduced by spectral multiplexing (compressed detection) using digital micromirror devices or by using SPAD arrays.

Keywords: Raman spectroscopy, medical diagnosis, time-gated, skin cancer, basal cell carcinoma

(Some figures may appear in colour only in the online journal)

1. Introduction

Raman spectroscopy is a powerful analytical technique for label-free molecular analysis of tissue [1] and has been widely used for medical applications [2]. Several Raman devices have been tested in hospitals for improving diagnosis

and treatment: hand-held Raman probes for *in-vivo* cancer diagnosis [3, 4], detection of residual tumour during cancer surgery [5], bone disease [6], Raman endoscopes [7–9], or *ex-vivo* Raman needle-probes [10–12] and multimodal Raman-autofluorescence (AF) [13–15] to assess completeness of tumour excision during cancer surgery. When acquiring Raman spectra of biological samples, it is important to block any stray or ambient light from reaching the detector as this background signal can swamp the tissue specific Raman bands. While this aspect is less relevant for *ex-vivo* tissue analysis (as the sample can be placed inside a light-tight instrument [16]) or for *in-vivo* applications where the probe can be brought in close contact with or inserted into the tissue,

* Author to whom any correspondence should be addressed.



Original content from this work may be used under the terms of the [Creative Commons Attribution 4.0 licence](https://creativecommons.org/licenses/by/4.0/). Any further distribution of this work must maintain attribution to the author(s) and the title of the work, journal citation and DOI.

ambient light can be a big challenge for the Raman measurements. When such light-tight conditions cannot be achieved, performing Raman measurements would typically require the lights in the operating theatre to be turned off. Even for endoscopic Raman probes it may be advantageous to maintain the visible light on to facilitate positioning the probe at a specific location, use near-infrared (NIR) light guidance or to perform measurements using different imaging modalities simultaneously.

The effects of various sources of ambient light in an operating theatre on Raman spectroscopy has been previously evaluated by Desroches *et al* [4]. Using a handheld contact probe with IR guided neuronavigation they assessed the impact of ambient light during Raman analysis of brain tissue. It was shown that microscope lights, fluorescent lights and standard operating room lights pointed at the sample must be switched off or shielded during Raman acquisition. The large background from the neuronavigation IR source also led to detector saturation. While the high concentration of lipids in brain tissue resulting in a relatively strong Raman signal mitigated some of these drawbacks, for weaker Raman scatterers such as skin, the effect of ambient lighting can have greater impact on the signal.

Background removal can be performed computationally or experimentally. Effective background subtraction techniques such as polynomial fitting [17] can be applied quickly to large hyperspectral datasets with minimal user input. More recent developments have utilised artificial neural networks to negate the effects of various light sources on Raman spectroscopy in an operating theatre [18].

An effective experimental method of removing background exists in shifted excitation Raman difference spectroscopy. The difference between Raman spectra taken at two different excitation wavelengths yields a spectrum free from both broadband backgrounds and backgrounds with sharp spectral features such as those generated from fluorescent or LED lighting. A recent development utilising custom charge-coupled device (CCD) hardware and software uses a novel charge shifting technique to improve acquisition speed and account for rapidly varying backgrounds that might be found in the field or in real world spectroscopy applications [19, 20]. If, however, the detector becomes saturated or the photon shot noise of the background is of the order of the signal, the effectiveness of such techniques diminishes. In such a situation it is desirable to separate the sources of the incoming signal.

Time-gated (TG) Raman spectroscopy utilises a pulsed laser excitation and detection system with high temporal resolution to provide an additional temporal dimension [21]. As Raman scattering can be considered instantaneous, the Raman signal will closely follow the temporal response of the laser pulse. As fluorescence typically operates on a nanosecond timescale, and many sources of noise and background are continuous, operating in the time domain allows one to separate the Raman signal from other sources of light and noise more effectively.

Usually employed to provide suppression of fluorescence backgrounds [22–25], the added temporal dimension yields

information on photon time of flight, Raman scattered photon diffusion times and fluorescence lifetimes.

There are two main techniques used to provide this additional temporal dimension, gating and time-correlated single photon counting (TCSPC). Gating involves optically (through the use of an optical Kerr gate) or electronically (controlling the accelerating voltage of a microchannel plate photomultiplier tube (MCP PMT)) gating the signal, preventing photons or photoelectrons from reaching the detector. TCSPC makes use of a time to digital convertor (TDC) to measure the difference between a detection event and a laser sync pulse. Each detection event is assigned a time tag and stored into memory.

For every period between laser pulses T , the detection method is configured to only acquire photons from a small window known as the ‘gate’ window of a width t_g . Photons incident on the detector that lie outside of the gate window will not be detected and thus would not contribute to the total signal. Provided the laser excitation pulse and the temporal resolution of the instrument is less than the gate window, the total possible background suppression is given by the ratio of the time gate to the period of the laser pulse T/t_g .

Acquisition of Raman spectra under ambient light conditions has been reported for stand-off Raman applications based on pulsed lasers and TG detection using intensified CCDs (iCCD) [21], which rely on an MCP PMT. iCCDs are relatively easy to implement, have high repetition rates of up to 100 MHz with a intensifier gate width as short as 250 ps [26]. However, iCCDs have a number of drawbacks when used for biomedical applications of Raman spectroscopy. Because many tissue types exhibit large levels of AF when excited by lasers with wavelengths in the visible range, lasers in the near-infrared region are used (above 750 nm wavelength). In the region 800–900 nm region corresponding to the fingerprint Raman region when using 785 nm excitation, the quantum efficiency of an iCCD (S20 photocathode) is approximately 0.20% [27]. While TG Raman spectra using iCCD have been reported using 720 nm laser excitation, the materials investigated (minerals [26], polymers and explosives [28]) had much higher Raman scattering cross-sections compared to typical biological tissue samples. Another potential drawback is that iCCDs require a fixed time gating window of a specific width determined by either software or by fixed experimental parameters. Variations of the distance between the probe and sample or photon diffusion times can lead to loss of signal. Multiple measurements must therefore be made with varying delays to acquire the complete photon distribution.

In this paper we show that TG Raman spectroscopy using a single photon avalanche diode (SPAD) operating in TCSPC mode is an alternative approach that can overcome these limitations. As the detector is a single channel detector, a scanning monochromator is used to record a Raman spectrum. In recent years, SPADs have become commercially available with high temporal resolution and detection efficiencies almost equivalent to the best research level CCD detectors. They have been shown to be effective for fluorescence suppression in Raman spectroscopy [18, 20], molecular depth

analysis of optically turbid materials based upon photon time of flight [29], and TG Raman mapping of materials eliciting strong fluorescence backgrounds when combined with spectral multiplexing (or compressed detection) [25]. Here, we investigated the use of this time-modulated Raman spectroscopy technique for measuring single-point Raman spectra and Raman raster maps of biological tissue samples.

2. Materials and methods

2.1. Materials

Human skin tissue containing basal cell carcinoma (BCC) were obtained from a patient undergoing Mohs micrographic surgery at the Nottingham NHS Treatment Centre. For this proof-of-concept work, only one sample was investigated that measured approximately 10 mm × 10 mm × 3 mm thickness. Ethical approval was granted by the Nottingham Research Ethics Committee (07/H0408/172). Informed consent was obtained from the patient. After surgical excision, the tissue specimen was embedded within optimal cutting temperature medium and frozen with a cryogenic spray (Frostbite, Surgipath). The specimen was sectioned according to Mohs micrographic surgery standard operating procedure. A 10 μm thick section was cut from the tissue (called adjacent section) and was stained by haematoxylin and eosin (H&E) and used as the standard of reference. Samples were then defrosted, washed and kept frozen at −20 °C until used for measurements. Porcine tissue (abdomen region, containing muscle and adipose tissue) was obtained from a local supermarket. An optically clear polystyrene petri dish from Sigma-Aldrich was used for initial experiments and calibration (Raman shift frequency standard, ASTM 1840 [30]).

2.2. Instrumentation

A schematic description of the instrument is presented in figure 1(a). A Nikon Eclipse inverted microscope was used to excite and collect the Raman scattered light. The beam of a pulsed laser (Katana 775, OneFive, 775 nm, 50 mW average power, 30 ps pulse width at 10 MHz repetition rate) is directed into the microscope via the dichroic mirror (DM) where it was focused onto the sample placed on a motorised translation stage via an objective (Leica 50×). Backscattered (also any fluorescence and background) photons were collected by the objective, the collimated light passed through the DM and the long pass filter before being focused onto the entrance slit of the spectrometer. A Czerny–Turner spectrometer (Andor Shamrock 303i) was used to disperse and focus the spectrum. The spectrometer included a motorised grating and flipper mirror to direct the spectra on a CCD (Andor DU401) or the SPAD. Two SPADs were used in this work; the PDM 100CTE from micro photon devices (instrument response function (IRF) 65 ps full width half maximum (FWHM), 10% detection efficiency@820 nm) and the COUNT-T from Laser Components (IRF 450 ps FWHM, 70%

detection efficiency@820 nm). The logic level digital pulses from the SPAD and the laser sync output were compared using a low-cost TDC (GPX2, Scio Sense) with 10 ps resolution. A microcontroller was programmed to configure the TDC, receive data via serial peripheral interface (SPI) and compress the data by binning into 5 ps binned histograms. The resulting histogram is sent to MATLAB via serial at the end of each acquisition period for storage and analysis.

3. Results and discussion

3.1. Instrument optimisation

In this study we included two SPADs: the PDM100CTE model provides higher temporal resolution (65 ps) but lower quantum efficiency (10%), and Laser Components Count-T model with poorer temporal resolution (450 ps) but a much higher quantum efficiency in the near-infrared region of interest (70% in the 800–900 nm range). The use of near infra-red excitation was required in order to minimise tissue AF background which can swamp the Raman bands. For each SPAD, the IRF was obtained by measuring the Raman signal generated by an optically clear polystyrene petri dish (figure 1(b)). The FWHM of the photon distribution measured by the SPAD provided a true measure of the instruments temporal resolution as it was the convolution of the laser pulse width, detector resolution and instrument parameters. For this instrument, the detector resolution was the dominating factor affecting the temporal resolution. In the case of TCSPC, the desired gate width and position can be applied post acquisition. Scatter plots representing each detection event for a sample with low background count (figure 1(c)) and a strong background count (figure 1(d)) better represents the potential advantages of this method. The high density of detection events at 83 ns corresponds to the Raman signal, all other detection events can be excluded and therefore their noise contributions are eliminated.

To determine the potential advantage of time gating over continuous wave (CW) wave Raman spectroscopy, a sample of transparent polystyrene was measured by both techniques with and without a strong background light source (microscope halogen lamp). Polystyrene was chosen for this task because it has a high Raman scattering cross section, its bands are stable and easily identifiable and is often used as a Raman frequency shift standard [30]. Figure 2 presents the results obtained using a CCD and the PDM100CTE detector (used initially for its superior temporal resolution). All data is presented as raw, unprocessed data with the exception of time gating applied post acquisition. TG Raman spectra acquired both with the halogen lamp on then switched off are presented in figures 2(c)–(j). With the halogen light off and sample cover closed, the Raman spectrum of polystyrene acquired using CW laser and CCD (figure 2(a)) shows all the characteristic Raman bands in agreement with [30]. With the cover removed, the intensity of the overhead halogen lamp was increased until the Raman bands could no longer be discriminated (figure 2(b)). The spectrum was then diverted to the side port via the spectrometers internal flipper mirror to acquire TG Raman spectra

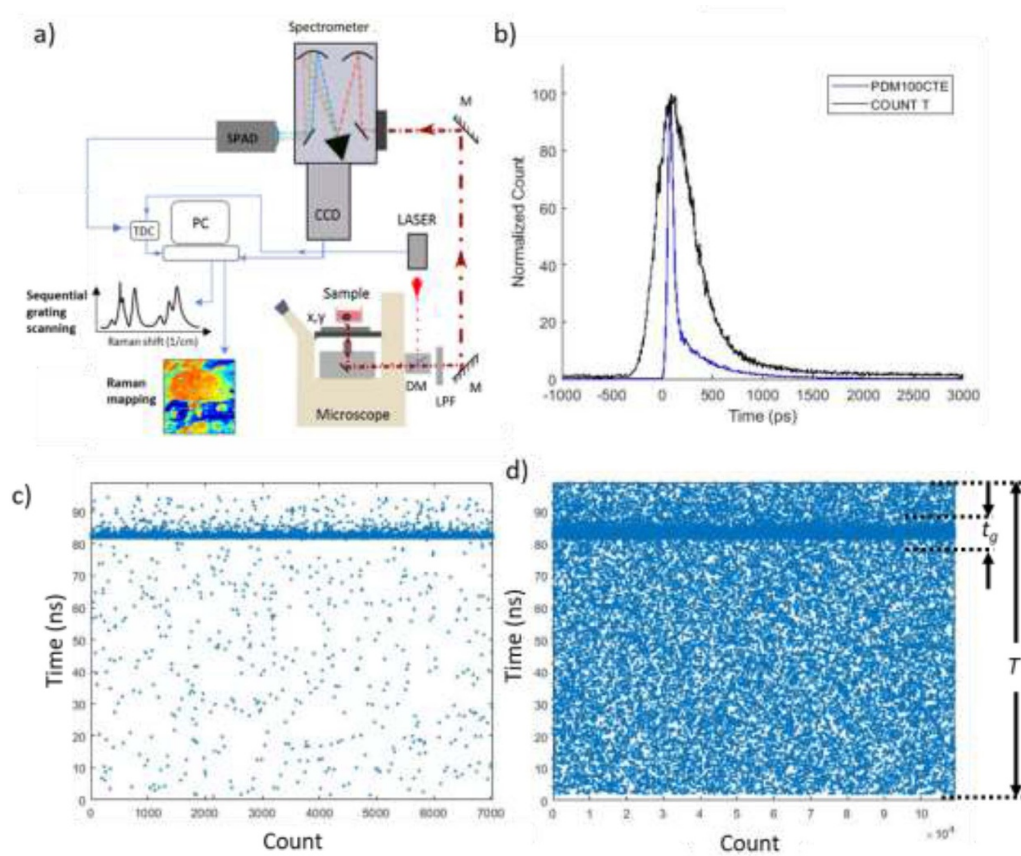


Figure 1. (a) Instrument schematic. The pulsed laser irradiates the sample mounted on an inverted optical microscope. Light collected by the objective passes through the dichroic mirror (DM), long pass filter (LPF) and is focused onto a fibre optic that is connected to the entry port of the spectrometer. The spectrum is focused onto the CCD or the single photon avalanche diode (SPAD). The digital outputs from the SPAD and laser are compared with a time to digital converter (TDC). (b) Instrument response functions (IRFs) of the PDM100CTE and the COUNT-T SPADs. IRFs were measured by acquiring the Raman scattered light from a transparent non-fluorescing polystyrene sample. (c), (d) Scatter plots of multiple detection events for a signal with low (c) and intense (d) continuous light background.

using the SPAD. The grating was scanned, and the spectrum was constructed from 500×1 s acquisitions. At each spectral position, a histogram was generated, and the desired time gate was applied post acquisition. The start position of the time gate was set to approximately 20 ps before the first Raman photons were detected. The closing position of the time gate window is indicated in figure 2. Figures 2(c)–(f) show TG Raman spectra for a selection of time gate windows with the sample covered and the lamp off. The results show that the TG Raman spectra are similar to the CW spectrum (figure 2(a)): all bands were detected and at the correct relative intensity. Figures 2(g)–(j) present the TG Raman spectra for the same time gate windows measured when the halogen lamp was switched on. While the lowest background level was observed at 100 ps, the optimal signal to noise ratio was found to be around 200–300 ps. To understand this effect, figure 3(a) shows the integration of the Raman signal over time. At 100 ps (indicated by the red cross) only $\sim 45\%$ of the total Raman signal is accounted for and it takes an approximately 200 ps window to account for the full distribution of photons (green cross). It should be noted that the trailing edge of the distribution is due to an effect inherent to SPADs known as afterpulsing and any further increase in

signal after 300 ps is due to the detector afterpulsing and not incident photons.

The signal to noise ratio in the Raman spectra was evaluated at each time gate using the intensity of the 1602 cm^{-1} Raman band and the rms noise in the $1480\text{--}1560 \text{ cm}^{-1}$ background region. Measurement of the background ($1480\text{--}1560 \text{ cm}^{-1}$) vs gate width shows the expected linear response (figure 3(c)) for a continuous background with no detector saturation. Figure 3(d) shows that optimum SNR occurs between 200 and 300 ps, corresponding to minimum width window that contains all Raman photons. For the 10 MHz repetition rate pulsed laser ($T = 100 \text{ ns}$) and a 200 ps width of the time gate, the effective background suppression factor of T/t_g is therefore $500\times$.

When using a CCD, strong background lighting can reduce the Raman SNR due to both the etaloning effect and photon shot noise. The results show that in the CCD limit of detection, a reduction in the background level by $\sim 100\times$ via time gating can yield spectra with an acceptable SNR. This suggests that for this system, adequate suppression of ambient light may be achieved using a gate width of 1000 ps and still provide a signal to noise advantage over a CCD detection system.

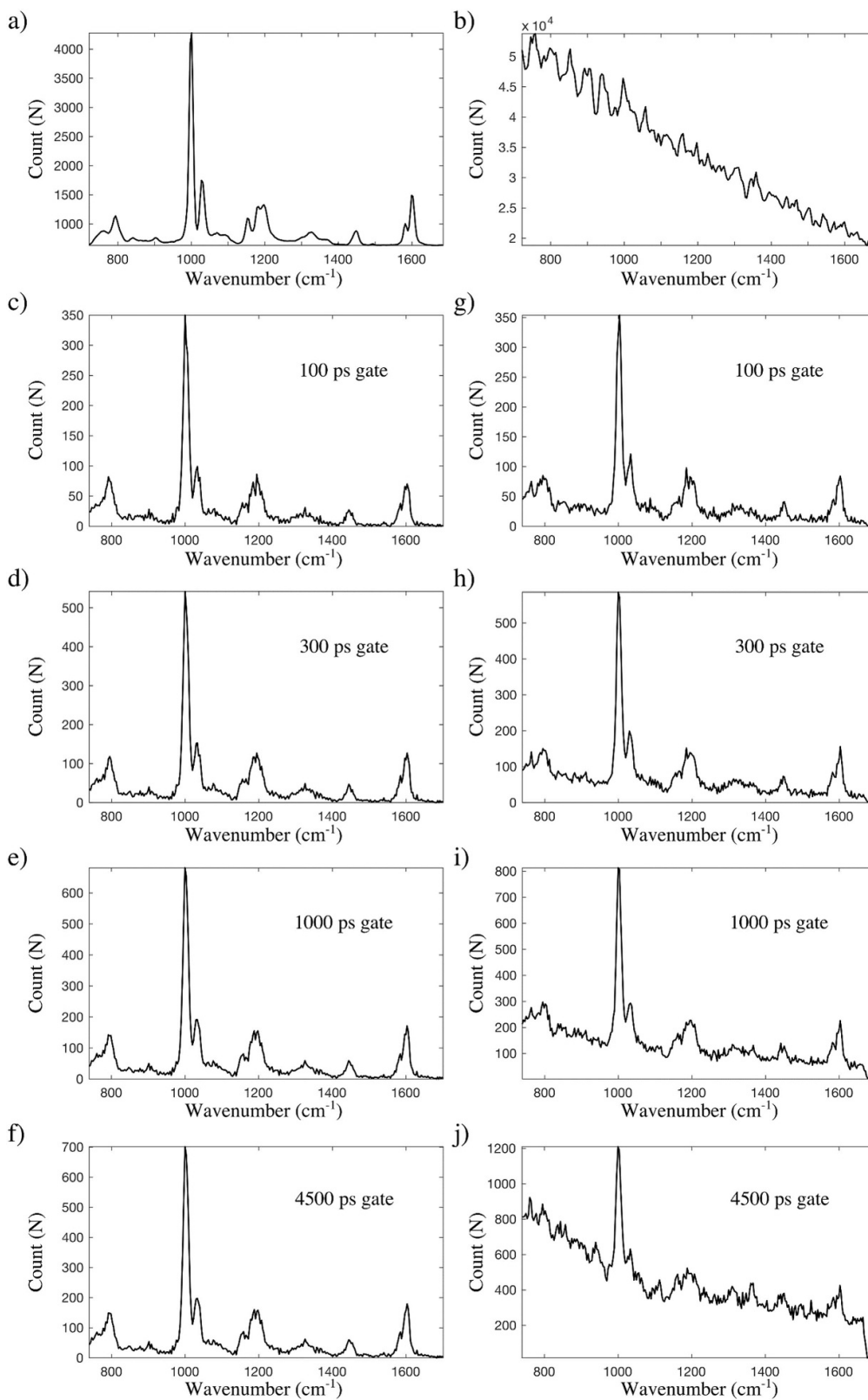


Figure 2. Raman spectra of polystyrene with background light off (a) and on (b) measured using the CCD detection. Time-gated Raman spectra of the same sample, at selected time gate windows, with background light off (c)–(f) and on (g)–(j).

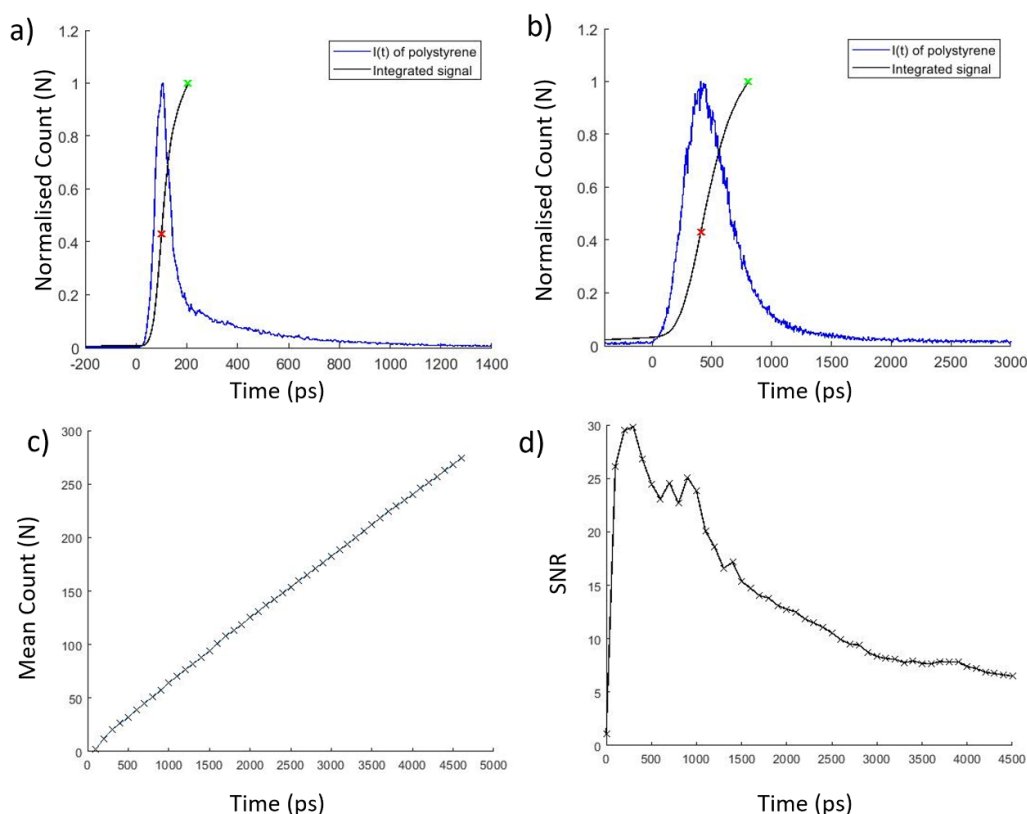


Figure 3. (a), (b) IRF and integrated Raman signal from clear polystyrene sample dish using PDM100CTE SPAD with 50 ps temporal resolution (red cross represents the 100 ps time point) (a) and the COUNT-T SPAD with 450 ps temporal resolution (red cross represents the 800 ps time point) (b). The green crosses represents the points when 100% of Raman photons are acquired; (c) average background count of polystyrene 1480–1560 cm^{-1} region with lights on vs time gate; (d) signal to noise ratio vs time gate width for polystyrene sample with lights on. Signal to noise evaluated from the 1602 cm^{-1} Raman band and associated 1480–1560 cm^{-1} background region.

Hence the COUNT-T SPAD with its seven-fold higher detection efficiency may be more suitable for applications where the low Raman scattering is the limiting factor. The low temporal resolution (450 ps) should still allow for greater than 100 \times suppression of ambient lighting using a 10 MHz pulsed laser, as long as a sample shows only low levels of AF. The IRF of the COUNT-T SPAD and integrated signal from a clear polystyrene Petri dish is shown in figure 3(b), indicating that a gate window of 800 ps (green cross) is required to account for all Raman photons, hence optimum SNR.

3.2. TG Raman spectroscopy and mapping of biological tissue

As biological samples typically have significantly lower Raman scattering cross-sections than common polymers, the PDM100CTE detector was replaced with the COUNT-T SPAD due to its >70% photon detection efficiency (PDE) (at 820 nm). The first evaluation experiments were carried out using porcine tissue using the CW and TG Raman conditions while illuminated with a broad band light source. The sample was approximately 10 \times 10 mm² (\sim 3 mm thick) and consisted of approximately equal parts of muscle and adipose tissue, as identified visually (figure 4(a)). This was confirmed by measuring an AF intensity image of the sample using the

775 nm laser as the excitation source and detection at 820 nm using the spectrometer and SPAD. The AF maps were generated by raster scanning the sample in the x - y plane using the motorised stage (0.1 mm step size) and 200 ms dwell time per pixel. Figure 4(b) shows that muscle is characterised by higher AF intensity compared to adipose tissue, likely due to the porphyrins in blood degradation products. The AF image was then used to select locations for Raman spectroscopy measurements, using both CW and TG modalities. Figure 4(c) shows the raw unprocessed CW Raman spectra (1 s integration time at 45 mW average laser power) acquired at the three positions indicated in figure 4(b) when the background light was off. Positions indicated by the green circle and the yellow square correspond to regions of adipose tissue and the Raman spectra are characterised by intense bands assigned to C-H, C-C and C=C vibrations (1070 cm^{-1} , 1301 cm^{-1} , 1450 cm^{-1} , \sim 1660 cm^{-1}) and typically found in adipose tissue [31]. The spectrum measured at the position indicated by the red star corresponds to muscle and consists only of a large AF background with no detectable Raman bands. When the halogen light was turned on, the Raman bands in all measured CW spectra were swamped by the background light (figure 4(d)).

Figure 4(e) presents the unprocessed TG Raman spectra acquired at the same locations using the SPAD with a 1000 ps

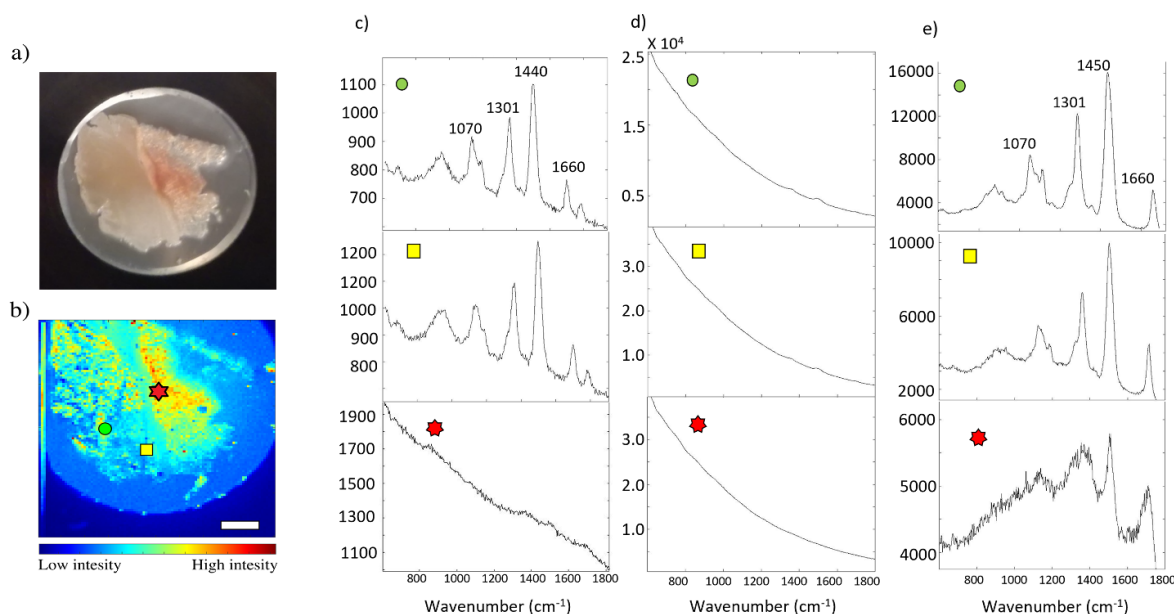


Figure 4. (a) Brightfield image of a porcine sample consisting of adipose and muscle tissue. (b) Near-infrared autofluorescence (AF) image at 820 nm emission. Symbols indicate the positions where point Raman spectra were collected for panels (c)–(e). Scalebar: 2 mm. (c) CW Raman spectra at selected positions measured with background lights off (1 s integration time). (d) CW Raman spectra at selected positions measured with background lights on (1 s integration time). (e) Time-gated Raman spectra at the same locations with background light on (3 s integration time per wavenumber). For all measurements, the average laser power was 45 mW. All spectra are presented raw (as measured) un-processed but shifted vertically for clarity, with the vertical axis representing the photon count (arbitrary units).

gate width and by sequentially scanning the diffraction grating to cover a spectral range similar to the CCD. Each spectrum was constructed from 500×3 s integrations at 45 mW average laser power. The data in figure 4(e) shows that the TG Raman spectra at locations corresponding to adipose tissue (circle and square), measured with the halogen lamp on, contain all Raman bands and at the correct relative intensity as measured with the CW conditions with the lights off. Raman bands of muscle tissue (red star) were also detected: amide I (1660 cm^{-1}) and amide III ($1200\text{--}1400 \text{ cm}^{-1}$), CH deformation (1450 cm^{-1}), ring breathing mode of phenylalanine (1002 cm^{-1}) [31].

Considering the high signal-to-noise ratio achievable for the TG Raman spectra, we investigated further the feasibility of recording Raman maps of tissue specimens under ambient light conditions. The sample presented in figure 4 was raster scanned using the motorised translation stage to generate 100×100 pixels Raman maps ($100 \mu\text{m}$ steps, with 200 ms integration time per pixel). As the instrument consisted of a single pixel detector, two separate maps were recorded at different wavenumbers. In order to enable Raman contrast between adipose tissue and muscle based, one map was recorded at 1450 cm^{-1} (CH_2 deformation band) and another at 1360 cm^{-1} (background). The generated Raman maps corresponding to different time gate windows of 600 ps, 1000 ps and 8000 ps are presented in figure 5. Because of the high AF background of muscle tissue, the map generated by the Raman bands at 1450 cm^{-1} (figure 5(a) (I_{1450})) does not discriminate well between the two tissue types as the signal is dominated by AF rather than the desired Raman intensity. However, after subtraction of the background map (figure 5 (I_{1360})), the

calculated difference Raman maps identify the adipose tissue with high contrast. Increasing the width of the time-gate to 1000 ps (figure 5(b)) has only a slight decrease in contrast compared to 600 ps (figure 5(a)), but extending the gate further (e.g. 8000 ps in figure 5(c)) leads to a significant drop in contrast.

3.3. Discrimination between cancer and normal tissue using TG Raman spectroscopy

Last we investigated the feasibility of TG Raman microscopy to detect, under high background light conditions, spectral differences in human tissue that would allow disease diagnosis. As an example, we selected BCC, which is the most common type of cancers in humans [32]. While Raman spectroscopy has been widely used for discrimination between normal tissue and cancer [2], including BCC [14, 16], we are not aware of any reports using TG Raman spectroscopy. Previous studies showed that Raman spectra of BCC are characterised by higher signals assigned to nucleic acids and lower intensity bands of collagen compared to Raman spectra of dermis in normal skin [33].

Figure 6(a) presents the adjacent histology-stained section of a typical skin tissue containing BCC investigated by the CW and TG Raman spectroscopy, with and without background light. As the Raman analysis was carried out on the unstained tissue sample, the adjacent stained H&E section allowed, by comparison, identification of BCC and normal dermis in the tissue (figure 6(a)). The tissue sample used for Raman analysis was defrosted and mounted in a sample holder with a quartz window.

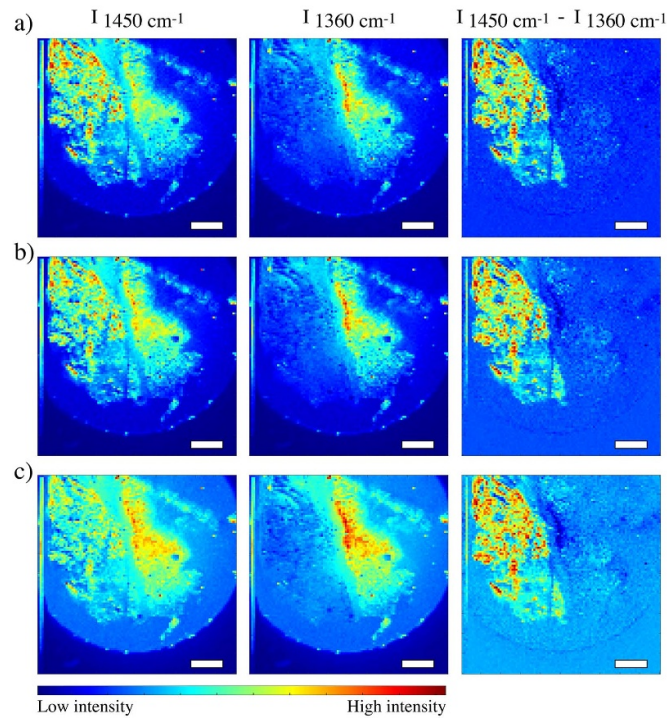


Figure 5. Raman maps of porcine tissue sample from figure 4 acquired with background light on for three different time gates: (a) 600 ps, (b) 1000 ps, (c) 8000 ps. Acquisition time 200 ms per pixel. Two maps were measured at each pixel, one for the 1450 cm^{-1} band and a second map for associated background level at 1360 cm^{-1} . The difference images ($I_{1450}-I_{1360}$) show the regions of high adipose tissue. Scalebars: 2 mm.

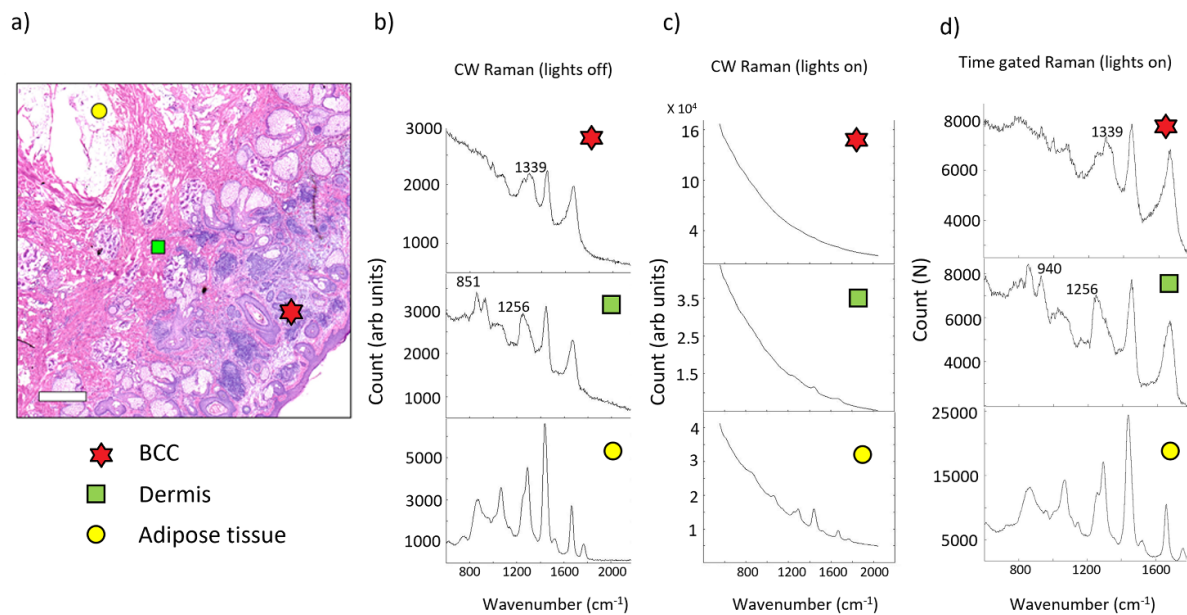


Figure 6. (a) Histology H&E stained section of skin tissue with adipose (yellow circle), dermis (green square) and BCC (red star). (b) CW Raman spectra with no background light acquired using CCD at 5 s integration with 45 mW excitation power. (c) CW Raman spectra with background light on, acquired using CCD at 5 s integration with 45 mW excitation power. (d) Time-gated Raman spectra with strong broadband background illumination; 3 s per wavenumber integration time, 1000 ps gate width at 45 mW. The Raman spectrum of quartz substrate was subtracted from all spectra (no other processing was applied). Scalebar: $500\ \mu\text{m}$.

Figure 6(b) presents CW Raman spectra, recorded with background light off at selected locations of the sample corresponding to normal dermis and BCC. In agreement with previous reports, Raman spectra of BCC was characterised by

stronger bands corresponding to DNA, such as PO_2 stretching at 1098 cm^{-1} and nucleic base ring stretching at 1339 cm^{-1} , as reported by previous studies [15, 16]. Spectra from dermis regions had spectral contributions from collagen, which is the

structural component of this tissue type. The three main bands specific to collagen at 851 cm^{-1} , 940 cm^{-1} and 1256 cm^{-1} correspond to proline, hydroxyproline and amide III, respectively [27]. When the halogen lamp was switched on, the background light swamped the Raman bands in CW mode (figure 6(c)). However, the time gating detection was efficient at suppressing the background light and all spectral features detected in the CW spectra with lights off were also detected in the TG Raman spectra under background lighting (figure 6(d)).

These results show that time gating Raman spectroscopy can be used for measurements of high-quality Raman spectra of biological samples suitable for medical diagnosis in optically noisy environments. The use of near-infrared excitation reduced the AF background from endogenous fluorophores present in many biological samples. This relaxes the temporal resolution required for effective ambient light suppression, enabling the use of detectors with higher quantum efficiency but lower time resolution. The results obtained using animals tissue samples (adipose tissue and muscle) showed that time gates of approximately 1000 ps enabled the measurement of Raman spectra under background light conditions of similar quality as conventional CCD detection Raman spectroscopy in the absence of background light. This proof-of-concept work shows that TG Raman spectroscopy is able to detect subtle spectral differences required for medical diagnostics, such as differences in Raman spectra of cancer and normal tissue in the presence of high levels of background light.

Although using a single pixel detector required longer acquisition times for grating scanning, the actual acquisition times per wavenumber were similar to CW. Compressive detection techniques using spatial light modulators have been shown to provide both speed and sensitivity advantages over CCDs in high and low signal regimes [34]. The combination of time gating with compressive detection offers a potential route to rapid classification of materials via Raman scattering in optically noisy environments. Alternatively, SPAD arrays would provide acquisition of TG Raman spectra without requiring grating scanning. While extensive progress has been made on SPAD arrays in recent years, there are still technical difficulties yet to be overcome such as low fill factor and low PDEs in the NIR regime (less than 12%) [35, 36].

4. Conclusions

This study demonstrates that TG Raman spectroscopy is a viable technique for medical applications for operation in the presence of high levels of background light. These include the need of maintaining ambient light conditions or when simultaneously being used with other optical modalities that overlap spectrally. The technique could well be effectively applied in many other areas such as manufacturing and industry. The compact nature of the SPAD and associated electronics would lend itself to a compact portable device that could be implemented in-field that is immune to a range of background sources.

Data availability statement

The data that support the findings of this study are available upon reasonable request from the authors.

Acknowledgments

This work was supported by the UK Engineering and Physical Sciences Research Council (Grant Number EP/L025620/1) and the UK Medical Research Council (Grant Number MC_PC_18058).

ORCID iD

Ioan Notingher  <https://orcid.org/0000-0002-5360-230X>

References

- [1] Shipp D W, Sinjab F and Notingher I 2017 Raman spectroscopy: techniques and applications in the life sciences *Adv. Opt. Photonics* **9** 315–428
- [2] Kong K, Kendall C, Stone N and Notingher I 2015 Raman spectroscopy for medical diagnostics—from *in-vitro* biofluid assays to *in-vivo* cancer detection *Adv. Drug Deliv. Rev.* **89** 121–34
- [3] Lui H, Zhao J, McLean D and Zeng H 2012 Real-time Raman spectroscopy for *in vivo* skin cancer diagnosis *Cancer Res.* **72** 2491–500
- [4] Desroches J et al 2015 Characterization of a Raman spectroscopy probe system for intraoperative brain tissue classification *Biomed. Opt. Express* **6** 2380
- [5] Jermyn M, Mok K, Mercier J, Desroches J, Pichette J, Saint-Arnaud K, Bernstein L, Guiot M-C, Petrecca K and Leblond F 2015 Intraoperative brain cancer detection with Raman spectroscopy in humans *Sci. Transl. Med.* **7** 274ra19
- [6] Buckley K, Kerns J G, Vinton J, Gikas P D, Smith C, Parker A W, Matousek P and Goodship A E 2015 Towards the *in vivo* prediction of fragility fractures with Raman spectroscopy *J. Raman Spectrosc.* **46** 610–8
- [7] Wang J, Lin K, Zheng W, Ho K Y, Teh M, Yeoh K G and Huang Z 2015 Simultaneous fingerprint and high-wavenumber fiber-optic Raman spectroscopy improves *in vivo* diagnosis of esophageal squamous cell carcinoma at endoscopy *Sci. Rep.* **5** 1–10
- [8] Bergholt M S, Zheng W, Ho K Y, Teh M, Yeoh K G, So J B Y, Shabbir A and Huang Z 2013 Fiber-optic Raman spectroscopy probes gastric carcinogenesis *in vivo* at endoscopy *J. Biophoton.* **6** 49–59
- [9] Almond L M et al 2014 Endoscopic Raman spectroscopy enables objective diagnosis of dysplasia in Barrett's esophagus *Gastrointest. Endosc.* **79** 37–45
- [10] Day J C C and Stone N 2013 A subcutaneous Raman needle probe *Appl. Spectrosc.* **67** 349–54
- [11] Jensen M, Horgan C C, Vercauteren T, Albro M B and Bergholt M S 2020 Multiplexed polarized hypodermic Raman needle probe for biostructural analysis of articular cartilage *Opt. Lett.* **45** 2890–3
- [12] Stevens O, Petterson I E I, Day J C C and Stone N 2016 Developing fibre optic Raman probes for applications in clinical spectroscopy *Chem. Soc. Rev.* **45** 1919–34
- [13] Shipp D W, Rakha E A, Koloydenko A A, Macmillan R D and Ellis I O 2018 Intraoperative spectroscopic assessment of surgical margins during breast conserving surgery *Breast Cancer Res.* **20** 69

- [14] Boitor R *et al* 2021 Clinical integration of fast Raman spectroscopy for Mohs micrographic surgery of basal cell carcinoma *Biomed. Opt. Express* **12** 2015–26
- [15] Kong K, Rowlands C J, Varma S, Perkins W, Leach I H, Koloydenko A A, Williams H C and Notingher I 2013 Diagnosis of tumors during tissue-conserving surgery with integrated autofluorescence and Raman scattering microscopy *Proc. Natl Acad. Sci.* **110** 15189–94
- [16] Boitor R *et al* 2017 Automated multimodal spectral histopathology for quantitative diagnosis of residual tumour during basal cell carcinoma surgery *Biomed. Opt. Express* **8** 5749–66
- [17] M.-j. A and Lieber C A 2003 Automated method for subtraction of fluorescence from biological Raman spectra *Applied Spectrosc.* **57** 1363
- [18] Jermyn M, Mercier J, Tremblay M, St-arnaud K, Guiot M, Jermyn M, Desroches J, Mercier J, Tremblay M and St-arnaud K 2021 Neural networks improve brain cancer detection with Raman spectroscopy in the presence of operating room light artifacts *J. Biomed. Opt.* **21** 094002
- [19] Sowoidnich K, Towrie M and Matousek P 2019 Lock-in detection in Raman spectroscopy with charge-shifting CCD for suppression of fast varying backgrounds *J. Raman Spectrosc.* **50** 983–95
- [20] Sowoidnich K, Towrie M, Maiwald M, Sumpf B and Matousek P 2019 Shifted excitation Raman difference spectroscopy with charge-shifting charge-coupled device (CCD) lock-in detection *Appl. Spectrosc.* **73** 1265–76
- [21] van Duyne R P, Jeanmaire D L and Shriver D F 1974 Mode-locked laser Raman spectroscopy. A new technique for the rejection of interfering background luminescence signals *Anal. Chem.* **46** 213–22
- [22] Matousek P, Towrie M, Ma C, Kwok W M, Phillips D, Toner W T and Parker A W 2001 Fluorescence suppression in Raman spectroscopy using a high performance picosecond Kerr gate *J. Raman Spectrosc.* **32** 983–8
- [23] Kostamovaara J, Tenhunen J, Kögler M, Nissinen I, Nissinen J and Keränen P 2013 Fluorescence suppression in Raman spectroscopy using a time-gated CMOS SPAD *Opt. Express* **21** 31632–45
- [24] Efremov E V, Buijs J B, Gooijer C and Ariese F 2007 Fluorescence rejection in resonance Raman spectroscopy using a picosecond-gated intensified charge-coupled device camera *Appl. Spectrosc.* **61** 571–8
- [25] Corden C J, Shipp D W, Matousek P and Notingher I 2018 Fast Raman spectral mapping of highly fluorescing samples by time-gated spectral multiplexed detection *Opt. Lett.* **43** 5733
- [26] Hooijschuur J H, Iping Petterson I E, Davies G R, Gooijer C and Ariese F 2013 Time resolved Raman spectroscopy for depth analysis of multi-layered mineral samples *J. Raman Spectrosc.* **44** 1540–7
- [27] Selb J, Joseph D K and Boas D A 2006 Time-gated optical system for depth-resolved functional brain imaging *J. Biomed. Opt.* **11** 044008
- [28] Iping Petterson I E, López-López M, García-Ruiz C, Gooijer C, Buijs J B and Ariese F 2011 Noninvasive detection of concealed explosives: depth profiling through opaque plastics by time-resolved Raman spectroscopy *Anal. Chem.* **83** 8517–23
- [29] Corden C, Matousek P, Conti C and Notingher I 2021 Sub-surface molecular analysis and imaging in turbid media using time-gated Raman spectral multiplexing *Appl. Spectrosc.* **75** 156–67
- [30] ASTM 2007 *Standard Guide for Raman Shift Standards for Spectrometer Calibration* (American National Standards Institute) (available at: <https://webstore.ansi.org/Standards/ASTM/ASTME1840962014>)
- [31] Tu A T 1982 *Raman Spectroscopy in Biology: Principles and Applications* (A Wiley-Interscience Publication) (New York: Wiley)
- [32] Fitzmaurice C, Abate D, Abbasi N, Abbastabar H, Abd-Allah F, Abdel-Rahman O, Abdelalim A, Abdoli A, Abdollahpour I and Abdulle A S M 2019 Global, regional, and national cancer incidence, mortality, years of life lost, years lived with disability, and disability-adjusted life-years for 29 cancer groups, 1990–2017: a systematic analysis for the global burden of disease study *JAMA Oncol.* **5** 1749–68
- [33] Larraona-Puy M, Ghita A, Zoladek A B, Perkins W, Varma S, Leach I H, Koloydenko A, Williams H and Notingher I 2009 Development of Raman microspectroscopy for automated detection and imaging of basal cell carcinoma *J. Biomed. Opt.* **14** 54031
- [34] Scotté C, de Aguiar H B, Marguet D, Green E M, Bouzy P, Vergnole S, Winlove C P, Stone N and Rigneault H 2018 Assessment of compressive Raman versus hyperspectral Raman for microcalcification chemical imaging *Anal. Chem.* **90** 7197–203
- [35] Bruschini C, Homulle H, Antolovic I M, Burri S and Charbon E 2019 Single-photon avalanche diode imagers in biophotonics: review and outlook *Light Sci. Appl.* **8** 87
- [36] Alayed M and Deen M J 2017 Time-resolved diffuse optical spectroscopy and imaging using solid-state detectors: characteristics, present status, and research challenges *Sensor* **17** 2115